Published in final edited form as:
*J Control Release*. 2012 December 10; 164(2): 236–246. doi:10.1016/j.jconrel.2012.10.007.

# Challenges and Opportunities in the Advancement of Nanomedicines

**Alexander Wei**[a], **Jonathan G. Mehtala**[a], and **Anil K. Patri**[b]

Alexander Wei: alexwei@purdue.edu; Anil K. Patri: patria@mail.nih.gov

[a]Department of Chemistry, Purdue University, 560 Oval Drive, West Lafayette, IN, 47907 USA

[b]Nanotechnology Characterization Laboratory, Advanced Technology Program, SAIC-Frederick, Inc., NCI-Frederick, Frederick, Maryland 21702 USA

## Abstract

Nanomedicine-based approaches to cancer treatment face several challenges that differ from those encountered by conventional medicines during clinical development. A systematic exploration of these issues has led us to identify the following needs and opportunities for further development: (1) robust and general methods for the accurate characterization of nanoparticle size, shape, and composition; (2) scalable approaches for producing nanomedicines with optimized bioavailability and excretion profiles; (3) particle engineering for maintaining low levels of nonspecific cytotoxicity and sufficient stability during storage; (4) optimization of surface chemistries for maximum targeted delivery and minimum nonspecific adsorption; (5) practical methods for quantifying ligand density and distributions on multivalent nanocarriers; and (6) the design of multifunctional nanomedicines for novel combination therapies with supportable levels of bioaccumulation.

### Keywords

nanomedicine; drug delivery; size analysis; pharmacokinetics; ligand density; active targeting; passive uptake

## Introduction

Nearly a decade ago, the U.S. National Institutes of Health announced a set of initiatives famously referred to as the NIH Roadmap, comprised of multidisciplinary research pathways with a mission to "dramatically change the content or the process of medical research in the next decade [1]." One such pathway resulted in the accelerated development of nanomedicine, broadly defined as "the design and application of nanoscale materials and metrologies for biomedical purposes [2]." Perhaps the largest and most active sector of research within this context has been the design of nanoengineered platforms for the targeted delivery and controlled release of chemotherapeutic agents. Many of these systems have been designed to take advantage of cellular uptake mechanisms that are not fully exploited by free drugs or traditional liposomes [3]. In addition, some carriers are equipped with



Correspondence to: Alexander Wei, alexwei@purdue.edu; Anil K. Patri, patria@mail.nih.gov.

functional nanomaterials to enhance imaging contrast, radiosensitivity, or localized hyperthermia for synergistic combination therapies [4, 5].

Novel nanomedicines and drug delivery systems continue to flourish in the research laboratory, with a commensurate increase in expectations of their clinical impact. So far, only a handful of "nanomedicines" have been approved by the U.S. Food and Drug Administration (FDA). These include: Doxil® and LipoDox®liposomal formulations of doxorubicin coated with polyethylene glycol (PEG) with diameters on the order of 100 nm [6, 7, 8]; Abraxane®an albumin-based suspension of paclitaxel with an average particle size of 130 nm, approved for the treatment of metastatic breast cancer [9, 10] and most recently Marqibo®liposomal particles containing vincristine sulfate with a mean size of 120 nm, for the treatment of acute lymphoblastic leukemia [11]. In addition to these marketed pharmaceuticals, an increasing number of nanoscale formulations have achieved investigational new drug (IND) status or are being evaluated in clinical trials (see Table 1 for selected examples) [12, 13, 14]. While many of these candidates are variants of previously established platforms, some recent entries are significantly different in composition or mechanism of action.

Despite these successful developments, most nanomaterials submitted for preclinical evaluation either have unacceptably high toxicities during *in vitro* or *in vivo* testing, or fail to meet the minimum criteria for bioavailability according to their adsorption, distribution, metabolism, and excretion (ADME) profile. The modest rate of success should be neither a surprise nor a source of pessimism; nevertheless, it is becoming clear that nanoengineered pharmaceuticals and drug delivery platforms have issues that are distinct from those of conventional pharmaceutical ingredients. Here we discuss several challenges and unmet needs facing nanomedicines during preclinical evaluation and early-stage clinical trials, and also address some issues concerning inorganic or metal nanoparticles with low excretion rates and long-term accumulation, and their potential to elicit a foreign body response.

## 1. Nanoparticle polydispersity: analysis

Particle size and shape are central to the pharmacokinetic properties of nanomedicines. The physical structure of nanoscale carriers can be optimized for extended blood circulation, efficient extravasation, or permeation through stromal tissue and the extracellular matrix [38, 39]. However, no single geometry is ideal for every stage of transport or delivery; for example, *in vitro* studies using colloidal gold (Au) nanoparticles indicated spheroidal 40–50 nm particles to be most effective for inducing receptor-mediated cell uptake and signal transduction [40, 41], whereas 20-nm PEG-coated Au nanoparticles were found to be most effective for permeating vascularized tumors by the enhanced permeation and retention (EPR) effect [42], with larger particles accumulating in the perivascular space [43]. Other studies involving the passive delivery of nanoparticles and macromolecules into tumor tissues suggest that particles in the size range of 10–12 nm offer the optimum balance between tissue penetration and overall retention [44, 45, 46]. Particle size and shape can also have variable effects on the behavior of macrophages and other cells following uptake [47, 48]. Macrophages can exhibit markedly different responses to different sized nanoparticles; in one study, phagocytosis of Au-coated nanospheres (ca. 30 nm) promoted cells to adopt a rounded, amoeboid morphology, whereas the uptake of nanostars (ca. 100 nm) induced the production of reactive oxygen species and pro-inflammatory agents such as TNF-α [49].

Particle size is also a major factor in excretion pathways (see Section 6 for further discussion). Solutes with a hydrodynamic diameter ($d_h$) below 10 nm tend to be eliminated rapidly through the kidneys (renal clearance), but larger colloidal species are filtered through the reticuloendothelial system (RES or hepatic clearance) and eventually eliminated through

the liver. In the example below, the clearance routes of MRI contrast agents based on PAMAM dendrimers were examined as a function of size, keeping all other parameters the same (Fig. 1) [50]. Dynamic MRI revealed that dendrimers up to the 6$^{th}$ generation ($d_h$ < 10 nm) were eliminated through the kidney (and thus suitable as renal contrast agents) while larger dendrimers were cleared through liver, with the route of clearance determined by a size difference of 2 nm. A pharmacokinetic study involving cysteine-coated CdSe–ZnS quantum dots revealed a similar size-dependent renal clearance, but with a lower threshold $d_h$ value of 5.5 nm [51]. It should be noted that the size threshold for renal clearance depends strongly on the architecture and deformability of the nano-carrier; in the case of polymeric nanostructures, branched architectures have much longer circulation times than linear ones, attributed to their reduced ability to reptate through nanosized pores [52].

The general importance of particle size and shape raises some questions whether nanomedicines can be characterized with acceptable levels of quality assurance and control. Unlike molecular entities, nanoparticles have an intrinsic polydispersity that is difficult to refine after synthesis. According to the National Institute of Standards and Technology (NIST)"a particle distribution may be considered monodisperse if at least 90% of the distribution lies within 5% of the median size," which translates into a relative standard deviation below 2% for Gaussian size distributions [53]. However, applying this definition to monodisperse *nano*particles is neither possible nor practical, because most available methods for nanoscale size analysis are insufficient to support this level of resolution, despite various refinements over the years.

The level of difficulty in characterizing particle size and polydispersity depends in part on material composition. For example, surfactant-stabilized inorganic and metal nanoparticles are easily characterized by transmission electron microscopy (TEM), thanks to their rigid structures and large electron scattering cross sections. On the other hand, electron microscopy is less straightforward for characterizing "soft" or "fuzzy" nanoparticles, such as polymer-coated nanocarriers or micelles that are easily deformed upon dehydration. TEM also has limited ability to provide real-time information on particle dynamics in liquid suspensions, such as their aggregation under physiological conditions.

With respect to practical size analysis, dynamic light scattering (DLS) is one of the more widely used methods in the characterization of nano-suspensions [54]. The $d_h$ values measured by DLS are frequently used to cross-validate those obtained by size-exclusion chromatography, which has limited resolution and dynamic range despite being the primary method of size analysis within the biopharmaceutical sector [55]. Methods based on field-flow fractionation and analytical ultracentrifugation (differential centrifugal sedimentation) are also useful for particle size analysis, but are more complex in operation and interpretation without significant benefits over DLS [56, 57, 58, 59]. DLS can produce data in a short period of time with a favorable level of accuracy (i.e. highly reproducible over multiple measurements), and offers the possibility of high throughput for quality analysis and control in production [55, 60]. DLS is also being applied toward analytical biosensing with picomolar sensitivity, based on a quantitative index of aggregation induced by proteins and other biomolecules [61].

DLS has several limitations as well. First and foremost, size analysis by DLS is based on particle ensembles, and the major distribution peaks can mask signals from small yet significant outlier populations. Second, despite its high accuracy, the precision of DLS is rather poor: while a 10% change in the $d_h$ peak position is sufficient for detecting aggregation [62], the peak width is broad with an effective resolution limit of 50% or more. Third, the size distributions are calculated from mathematical models based on the Brownian motion of isotropic (spherical) particles. The size distributions from such algorithms can be

skewed by shape anisotropy, and also tend to be weighted more heavily toward larger particles with stronger scattering signals, which scale roughly with $d^6$. This has a significant impact on the accuracy of size analysis, but can be corrected for by calculating an intensity-weighted size distribution, more commonly referred to as a Z-average.

In the example below, multiple batches of Au nanoparticles (produced with slight differences in procedure) were characterized by DLS and TEM (Fig. 2). The DLS mode intensities yield $d_h$ values that are systematically larger than those calculated by TEM image analysis, whereas the Z-average measurements are much closer. The comparison also reveals some limitations of DLS for routine measurements: while the standard (statistical) error of DLS is smaller than that obtained by TEM, the correlation of the two methods is not strong enough to support DLS as a stand-alone method of size analysis.

More precise analyses may be obtained by using single-particle measurement techniques such as scanning ion occlusion sensing (SIOS), which drives particulate analytes through a nanopore of tunable size [63, 64], or by nanoparticle tracking analysis (NTA), a method that employs video tracking and the Stokes–Einstein equation to convert particle diffusion rates into $d_h$ values [65, 66]. SIOS can reliably detect individual particles above 60 nm, whereas NTA can record the size of particles between 50–1000 nm (as small as 30 nm in the case of metal particles) at dilute concentrations ($10^7$–$10^9$ particles/mL), which is orders of magnitude lower than most DLS detection systems. NTA can also provide multimodal distributions, whereas size analysis by DLS is essentially unimodal. Furthermore, NTA is not strongly affected by size-dependent scattering intensities or aggregation: in a direct comparison between DLS and NTA, the size distributions of the latter are nearly Gaussian (Fig. 3) [65].

The resolution of NTA, SIOS, and several other single-particle counting methods were recently compared using colloidal silica, and found to be superior to DLS [67]. However, further development is needed before these methods can be fully embraced. In addition to their current size limits for particle detection, the sampling number for SIOS and NTA is relatively small ($N$ = 200–1000), resulting in greater statistical error. NTA is also sensitive to video recording parameters such as exposure and gain and requires some expertise for a reliable analysis. It is hoped that such technical challenges will eventually be resolved by further refinements in instrumentation and software. Given sufficiently high throughput, single-particle measurements may ultimately become the gold standard for the size analysis of nanoparticles.

Analysis of particle anisotropy is a more challenging issue than size dispersity, with fewer options for general users. While the issue of shape anisotropy has been recognized for some time [68], the increased dimensionality of particle analysis requires more complex, multi-parametric algorithms. Practical methods for morphology characterization are mostly limited to evaluations of shape ellipticity using 2D image analysis [69, 70]. In some cases, shape analysis can be performed on particle dispersions with low nanometer resolution using small-angle X-ray or neutron scattering (SAXS or SANS), but intensive computational modeling is still required [71]. However, it should be noted that new methods for particle shape analysis continue to emerge [72], with the potential to become practical technologies.

Lastly, size and shape analysis are just two of several structural characteristics that need to be addressed. Nanoparticles and nanocarriers of similar size and composition can still have important differences in ultrafine structure: a well-established example is the distinction between crystalline and amorphous nanocrystals, which can have very different rates of dissolution or degradation in physiologically relevant environments. In the example below, cryo-TEM analysis of commercial Doxil® particles (PEGylated liposomes loaded with

doxorubicin sulfate, 2 mg/mL) reveals this salt to deposit intravesicularly as crystalline nanorods that span the width of the particle, whereas PEGylated liposomes loaded with doxorubicin glucuronate do not demonstrate this tendency (Fig. 4) [8]. The latter has been tested in mouse tumor models and found to have a shorter circulation time than Doxil® but without loss of therapeutic efficacy, which may help to lower adverse side effects [73]. Such differences illustrate the importance of characterizing drug delivery vehicles with low-nanometer spatial resolution.

## Nanoparticle polydispersity: manufacturing

Scalability and batch-to-batch reproducibility present two significant barriers to the advancement of nanomedicines with novel architectures and compositions. Many promising leads are often based on nanomaterials prepared in batches of tens of milligrams, but there are far fewer reports of multigram syntheses of nanomaterials prepared with low (<5%) size polydispersity [74]. Multigram quantities of nanomaterials are necessary to perform quality preclinical evaluations for *in vivo* toxicological studies and ADME profiling, prior to filing for IND status, so batch-to-batch variations must be tightly controlled to meet safety standards.

Like any chemical reaction, process optimization for the scalable production of nanomaterials demands a considerable investment of time and effort. In the case of batch synthesis, nucleation and growth conditions for nanoparticles can be highly sensitive to reagent concentration, mixing rates, reaction volume and heat transport [75]. As an illustration, several batches of colloidal Au nanoparticles in our previously discussed example (Fig. 2A1–A4) were performed under seemingly identical conditions, yet their size distributions would be considered unacceptable from the perspective of quality control.

Continuous-flow (CF) reactors are widely used in the manufacturing of materials and chemicals because they allow for precise and programmable control over mixing rates, concentration, and pressure at a preset volume, which limits undesirable variations in heat or mass transfer. For the size-controlled synthesis of nanoparticles, CF microreactors have sub-millimeter channels to support laminar flow (low Reynolds number) conditions for rapid mixing and heat transfer rates. CF microreactors are capable of supporting multiple feed lines and high temperatures and pressures, and can produce composite particles with narrow size dispersities [76, 77]. When multiple CF microreactors are used in parallel, they can be competitive with batch reactors for scale-up. For example, it has been claimed that the production rate of phosphine-stabilized $Au_{11}$ clusters is 500 times faster using CF conditions versus conventional batch processing, when compared on the basis of reactor volume [78]. Colloidal Au particles can be prepared in the 5–50 nm range with polydispersities half that produced under conventional batch conditions [79]. Binary inorganic nanoparticles (e.g., semiconductor quantum dots) and metal-oxide nanoparticles have also been produced by CF as small as 1 nm, with size dispersities on the order of 6–10% [80].

With respect to monodisperse nanoparticles for drug delivery, the preparation of nanosized carriers using CF conditions remains an area in progress [81]. Polymeric micelles containing mithramycin have been made by a solvent exchange process with a mean diameter of less than 60 nm [82], and chitosan particles of controlled size have been prepared using spinning-disk processing, in either unloaded form ($d_h$ = 10–70 nm) or with low-molecular weight pharmaceutical ingredients (up to 400 nm) [83]. The anticipated advantage of producing nanocarriers by CF is the ease with which optimized conditions can be adapted for parallel processing for increased throughput. In this regard, it should be noted that alternatives to CF are also being developed, including the roll-to-roll synthesis of submicron polymer carriers using elastomeric templates (a.k.a. PRINT® technology) [84, 85], and the production of monodisperse microemulsions and capsules using microfluidic devices [86].

## 2. Surface chemistry and toxicity

The importance of surface chemistry in the biocompatibility of nanoparticles cannot be overstated, and has been addressed in several previous reviews [5, 14, 87, 88]. The most common concerns are (i) dispersion stability under physiological conditions; (ii) nonspecific cell uptake and cytotoxicity, and (iii) unfavorable biodistribution and clearance profiles. The first two issues can be evaluated readily *in vitro*, the former by optical analysis or imaging and the latter by standardized cell viability assays (e.g., MTT assays for mitochondrial activity, and LDH assays for membrane integrity). However, ADME characteristics are evaluated *in vivo* using small-animal models, which are often encumbered by high levels of variability and poor reproducibility between laboratories. Alternative models or methods for ADME evaluation are being actively discussed in several areas of pharmacology [89, 90, 91, 92, 93].

With regard to systemic toxicity, there has been increasing emphasis on the immunological effects of nanomedicines, which are taken up by macrophages residing in the liver and lymph nodes (Kupffer and dendritic cells) [94]. First, it is well known that many surface coatings or labels are immunogenic, so one must always be mindful of a strongly adverse immune response to nanoengineered particles. Second, surface charge (as determined by the particles' zeta potential at physiological pH) can be an important determinant of immunotoxicity, although not absolutely so; while cationic nanocarriers are often considered more likely to produce toxic effects than anionic particles (possibly for their tendency to promote protein aggregation and membrane permeation), there are many exceptions in each case [88, 95]. Particles coated with PEG or non-immunogenic polysaccharides have the best track record for minimizing immunotoxicity, but even these need to be thoughtfully designed to avoid negative interactions with the immune system (see Section 4) [94, 96, 97].

Many formulations are prone to changes in activity or potency upon prolonged storage. Nanomedicines are no exception; in fact, the problem may be compounded by issues of aggregation and leaching, which are ultimately determined by the qualities of their surface coatings. Long-term stability or shelf life is an issue that requires special attention, as studies on freshly prepared nanomedicines can produce very different activity profiles from those that have been stored for a few months. As a case in point, CTAB-stabilized Au nanorods (whose cationic quality facilitates their nonspecific cell uptake [98]) can be treated on a gram scale with sodium polystyrenesulfonate (PSS), then dialyzed exhaustively to produce nanorods with overall negative charge [99, 100, 101]. When freshly prepared, PSS-stabilized nanorods exhibited negligible cytotoxicity against mammalian cells; however, the same sample was discovered to be highly cytotoxic after less than 3 months of storage (Fig. 5). Remarkably, the PSS-treated suspension is even more cytotoxic than CTAB-stabilized nanorods prior to treatment, despite the fact that PSS is widely used in household and pharmaceutical products. The toxic component was deduced to be a PSS–CTAB complex that gradually leached from the nanorod surface, but could be removed by multiple centrifugation–redispersion cycles with fresh PSS to produce "CTAB-free" nanorod suspensions [99]. This toxicological study presents a simple solution that permits further preclinical studies with coated Au nanorods, but it serves as a reminder that long-term storage (shelf life) is also an important factor in the toxicological evaluation of novel nanomedicines.

## 3. Nonspecific adsorption versus targeted delivery

Protein adsorption and surface fouling are problems common to all materials and devices that come into contact with bodily fluids. In the case of nanomedicines, serum proteins can adsorb onto the particle surfaces (opsonization) to make them susceptible to phagocytosis,

and are largely responsible for their rapid removal from the bloodstream. Enormous efforts have been devoted toward the development of robust coatings that reduce nonspecific adsorption for extended circulation lifetimes, more efficient passive or active delivery, and minimal nonspecific cell uptake. For example, PEG-coated core–shell Au–$Fe_2O_3$ nanoparticles ($d$ ~10 nm) can be administered intravenously with a circulation half-life of 16 hours, enabling 15% or more of the injected dose per gram (ID/g) to accumulate in vascularized tumor tissues [102]. Larger Au nanoparticles and nanorods ($d$ > 50 nm) coated with linear or branched PEG derivatives can also have circulation times in excess of 24 hours [42, 103, 104, 105], but their passive uptake is less efficient (<7% ID/g) [106, 107, 108, 109].

One common problem in surface functionalization (particularly when using polymers such as PEG) is achieving an optimal chain density that discourages nonspecific adsorption or cell uptake while permitting targeted delivery. In the case of substrates with a high radius of curvature (i.e. microparticles or planar surfaces), PEG chains above a critical surface density (~1 molecule per 10 $nm^2$) can provide effective protein resistance when they adopt a brush-like conformation, assuming negligible interactions with the chain termini [110, 111]. Conversely, insufficient surface coverage produces less than optimal anti-fouling properties, and in some cases can even increase the surface absorption of certain types of proteins [112]. Methods for estimating the average density of PEG chains on particles exist, and can provide a practical index of surface coverage [113].

Nanoparticle–PEG interactions differ significantly from planar substrates because of their smaller radius of curvature, often within a few lengths of the adsorbed polymers [114, 115]. It is widely believed that at low surface density, hydrated PEG chains adopt a mushroom-like configuration with many PEG segments in local *gauche* conformations, which raises a significant entropic barrier to nonspecific protein adsorption (Fig. 6) [116, 117]. In the case of submicron liposomes, a small percentage of PEG derivatives (<5 wt%) is sufficient to inhibit protein-induced agglomeration and improve circulation lifetimes [118].

At higher density, PEG chains are expected to form polymer brush layers with extended chain conformations, which also provide a steric barrier to protein adsorption but may negatively affect the presentation of targeting ligands immobilized on the particle's surface [118]. This problem can be reduced by mounting ligands at the ends of PEG chains and at sufficiently low density to avoid opsonization, as has been shown in earlier studies using PEGylated liposomes with antibodies or antibody fragments (immunoliposomes) [119]. However, the issue of ligand presentation may be more persistent if the carrier size is further decreased. A recent study on RGD peptide-labeled nanoemulsions comprised of PEGylated phospholipid (PEG2000-DSPE, $d_h$ ~100 nm) suggests that targeting efficacy can still be negated by a high PEG density, even if the ligands are tethered at PEG termini (Fig. 6) [120].

It is worth noting that while active targeting can be used to increase the tumor cell uptake of nanomedicines *in vitro*, high-affinity ligands often do little to improve efficacy in systemic delivery and overall biodistribution *in vivo* [12, 121]. This is because the particles must first cross several physical barriers before reaching the surfaces of tumor cells [14]. The delivery of nanoparticles from the bloodstream to the targeted site is first determined by the efficiency of extravasation (e.g., the EPR effect), followed by their penetration into the tissue microenvironment. At this level, the bioavailability of nanomedicines depends strongly on their ability to navigate past the endothelial glycocalyx and extracellular matrix of the basement membrane [122], and also to overcome intrastitial fluid pressure gradients [38], prior to binding with their target receptors.

With respect to passive targeting, methods for functionalizing nanoparticles with protein-resistant PEG coatings still require careful optimization, despite some flexibility in design. Mono-functionalized PEG chains are generally grafted onto surfaces by a sequential adsorption process, but saturation coverage is not guaranteed even in the presence of excess ligand. Opsonization of poorly passivated nanocarriers not only affects the biodistribution but can also result in an immunotoxic response, even if the nanomaterials themselves are considered to have low intrinsic toxicity [94–97]. Examples of such adverse effects observed in animal (rat) models include pyrogranulomatous lesions in the lung and extensive pigmentation in the ovaries and muzzle [123]. Granulomatous lesions signify the presence of activated macrophages and the onset of a secondary immunotoxic response, when the initial inflammatory reaction (neutrophil recruitment) is insufficient to remove the inciting agent. Therefore, small differences in passivation conditions can have a dramatic effect on *in vivo* outcomes.

## 4. Characterization of multivalent nanoparticles

Many nanomedicines have been designed to present recognition ligands or antibodies for targeted delivery [29–33, 118, 124, 125, 126]. Nearly all of these systems are multivalent in nature, but very few analytical methods can quantify the precise density of targeting ligands per particle. Optimization of ligand density is largely based on the empirical results of *in vitro* biochemical or biological assays. Furthermore, the attachment of ligands onto particle surfaces by standard conjugate methods can be expected to produce a Poissonian distribution; for example, a single-particle fluorescence resonance energy transfer (FRET) study has shown that substoichiometric mixtures of ligand and quantum-dot nanoparticles will produce significant populations of unlabeled, monolabeled, and multivalent particles [127]. As a consequence, very few conjugated nanocarriers are prepared with sufficient control to permit a well-defined correlation between ligand density and increases in activity or bioavailability.

At the time of this writing, there is no universal method that can be applied routinely toward quantitative estimates of ligand density per particle, much less the distribution of multivalency in particle ensembles. Bulk sampling methods have been developed to provide an effective number average of ligands per particle: these include radiolabeling [113], the introduction or displacement of fluorescent labels [128, 129], colorimetric assays using ligand-specific dyes [130, 131], digestive peptide analysis [132], and multimodal analysis using mass spectrometry and NMR or other forms of spectroscopy [133, 134]. Quantitative methods based on matrix-assisted laser desorption ionization mass spectrometry (MALDI-MS) are now emerging; while most are only able to measure relative changes in surface density [135, 136, 137, 138], some are capable of producing absolute values when used with an isotopomer as a reference [139]. If charged ligands such as proteins are involved, electrospray–differential mobility analysis (ES-DMA) is a promising approach for measuring surface coverage on particles based on mass changes after surface adsorption [140, 141].

Functional atomic force microscopy (AFM) or spectroscopy is another potentially useful approach for quantifying the ligand density of individual nanoparticles. Samples can be dispersed onto planar substrates, then interrogated under solution by a probe tip functionalized with cognate receptors or antibodies [142, 143]. As the probe tip is withdrawn from the surface, ligand–receptor interactions are disrupted in a quantized fashion and registered by changes in mechanical force, which can be used to estimate the local ligand density. However, this method also has a number of liabilities. The serial nature of AFM limits the throughput of sample analysis, and the quality of biomolecular

recognition is sensitive to the placement and orientation of the receptor on the probe tip, which can be challenging to reproduce [144].

Ligand counting by AFM analysis also assumes that all surface molecules are accessible. However, the range of motion of the functionalized probe tip is restricted to a single, linear dimension, and the recognition ligand may be recessed or embedded within the particle coating, resulting in an artificially low count. In the example below, Au nanoparticles functionalized with the antigen TNF-α were further coated with PEG chains of variable length, then deposited onto a substrate and interrogated by a probe tip labeled with anti-TNF antibody. Multiple contact force measurements on TNF-labeled particles coated with 2-kDa PEG produced a mode peak centered around 180 pN, but the number of antigen–antibody binding force interactions decreased when the PEG size increased to 5 kDa, and completely disappeared in the presence of 20-kDa PEG (Fig. 7). In the latter case, only weak (ca. 20 pN) interactions were recorded, corresponding to nonspecific tip–PEG interactions. This study illustrates that PEG can mask biomolecular recognition, depending on its molecular weight. and that probe-based methods can be challenging to use for quantifying ligand-specific interactions on complex nanoparticle surfaces.

## 5. Bioaccumulation of nanomedicines

Numerous studies have shown that significant levels of nanomedicines administered systemically can accumulate in the lungs, spleen, kidneys, and liver, sequestered by macrophages residing in these organs or derived from the bone marrow. This applies to most materials over 10 nm (excluded from renal clearance), but also to smaller nanoparticles that are susceptible to opsonization or environmentally-induced agglomeration. A number of pharmacokinetic studies have established that neutral, PEG-stabilized particles below 100 nm provide the longest circulation times [43, 145, 146], although there are novel exceptions such as polymeric filomicelles, whose flow properties greatly reduce RES clearance by macrophage uptake with circulation times on the order of days [147, 148]. With respect to tumor penetration, we noted earlier that the optimal size range may be on the order of 10–12 nm [43–45], especially if the blood vessels can be normalized to reduce interstitial fluid pressure [46].

One approach for improving nanomedicine delivery to tumors (i.e., a higher % ID/g) is to increase the overall dosage in order to saturate the RES organs, thereby extending the clearance time. However, a primary concern for the accumulation of nanomedicines in untargeted cells and organs is the collateral release of cytotoxic materials that can lead to a wide range of adverse reactions in patients. Even FDA-approved formulations such as Doxil® and Abraxane® are far from optimal, with serious side effects such as neutropenia, hand–foot syndrome and other skin disorders, and cardiotoxicity [8, 9, 19]. Liver toxicity is the main reason for the failure of nanomedicines in clinical trials, although a recent study demonstrates significant size-dependent uptake by mesangial cells in the kidneys [149]. Toxic side effects in RES organs often define the maximum tolerated dose (MTD) in patients; clinical studies for any given formulation are likely discontinued if they do not show significant improvements in patient outcomes within the therapeutic window defined by the MTD.

The toxicities associated with most drug delivery platforms are acute, assuming that they are amenable to standard routes of excretion and elimination. However, inorganic or metal nanoparticles can have extremely low rates of excretion due to their intrinsic resistance to lysosomal degradation, resulting in long-term accumulation. In this context, indigestible nanomaterials may become a source of nonspecific cytotoxicity and inflammation, i.e. a foreign body reaction (such as the granulatomous lesions discussed in Section 3), an issue

that is now receiving considerable attention [47]. A well-studied example is the bioaccumulation of colloidal Au, which has been used in past decades for the clinical treatment of rheumatoid arthritis, and thus widely regarded as biocompatible [150]. While some circulating Au nanoparticles can be eliminated by hepatobiliary excretion [151], most end up in the spleen, liver, and mesenteric lymph nodes after hepatic clearance, where their degradation and excretion as ionic Au can take many months [152]. Internalized Au nanoparticles are also not easily eliminated from cells, despite some evidence for size-dependent exocytosis [153].

The bioaccumulation of metal nanoparticles presents a challenge to nanomedicine applications that seek to exploit their physical properties, namely their plasmon-enhanced optical and photothermal activities. The structures of Au nanoparticles can be engineered to produce plasmon resonances at near-infrared (NIR) wavelengths, considered by many to be ideal for biomedical imaging and theranostics [150, 154]. Many exciting proof-of-concept studies have been reported using NIR-active Au nanoparticles [101, 104, 107, 108, 155, 156, 157, 158], but most of these were performed at loadings of $10^2$–$10^3$ mg Au/kg tissue, which is too high to be considered bio-inert. A toxicological analysis of PEG-coated Au nanoparticles in mice ($d$ = 5–60 nm, ID = 4 mg/kg) indicated variable changes in white blood cell counts as well as liver and kidney damage, 28 days following intraperitoneal administration [96], and a study involving variable loadings of PEG-coated Au nanoparticles in mice ($d$ = 13 nm, ID = 0.17–4.26 mg/kg) indicated increasing levels of inflammation and apoptosis of hepatocytes, 7 days following intravenous administration [97]. A complementary study in rats has suggested that foreign body reactions can be caused by even lower levels of Au nanoparticles ($d$ = 20 nm, ID = 10 μg/kg) [159]. Genomic analysis of hepatocytes 2 months post-exposure revealed highly significant (>2-fold) changes in expression levels for nearly 80 genes: those that were upregulated included proteins associated with detoxification (P450), lipid metabolism (Sqle), and lymphocyte production (IL-7), while multiple proteins involved in the cell cycle process were downregulated.

The objective, then, should be to strike a balance between nanoparticle dosimetry and efficacy. In this regard, we note that the physical properties of metal or magnetic nanoparticles may be combined with other treatments to produce synergistic effects on therapeutic outcomes. Recent studies along these lines have shown that the photothermal properties of NIR-active Au nanoparticles can be used to trigger release from drug delivery vehicles [160, 161, 162, 163, 164] and can also sensitize cells to drug action by producing mildly hyperthermic conditions [165, 166, 167]. Similarly, magnetic nanoparticles can provide thermal or mechanical mechanisms for actuating drug release or sensitizing cells to chemotherapy [21, 168, 169, 170]. Nanomedicine platforms thus continue to hold much promise for designing combination therapies based on physical and chemical modes of action, but studies should also demonstrate efficacy without excessive loading.

## Conclusions

The prognosis for nanomedicine-based approaches toward cancer treatment is positive overall, but is tempered by anthropogenic limitations (i.e., compliance with regulatory and safety issues) as well as by biophysical ones. Currently available methods for nanomaterials characterization are not yet fully capable of providing a set of analytical standards that can reliably predict nanoparticle behavior based on size, shape, and surface composition, a vital need for both quality control and regulatory approval. The scalable production of nanomedicines with low size dispersity and uniform surface chemistry is another hurdle that must be surmounted prior to clinical trials. Formulations must also be optimized to provide sufficient control over nonspecific adsorption and ligand density, while maintaining therapeutically beneficial levels of targeting. Lastly, functional nanomaterials with novel

physical properties have the potential to transform cancer treatment when used in combination with conventional approaches, but should be designed to deliver significant improvements in outcome without creating a significant foreign body reaction. These diverse challenges create opportunities for developing better and more powerful methods for the analysis, production, and administration of cancer nanomedicines.

## Acknowledgments

The authors gratefully acknowledge support from the National Cancer Institute (RC1 CA-147096; the Lilly Endowment (College of Pharmacy), and the Purdue University Center for Cancer Research. We thank Henry Havel and David Thompson for helpful discussions and suggestions. This project has been funded in whole or in part with federal funds from the National Cancer Institute, National Institutes of Health, under Contract No. HHSN261200800001E. The content of this publication does not necessarily reflect the views or policies of the Department of Health and Human Services, nor does mention of trade names, commercial products, or organizations imply endorsement by the U.S. Government.

## References

1. Zerhouni E. The NIH roadmap. Science. 2003; 302(5642):63–72. [PubMed: 14526066]
2. Wei A. Focus on the Advances in Nanomedicine Symposium. 233rd National Meeting of the American Chemical Society, 2006. Nanomedicine. 2007; 2(1):83–83.
3. Torchilin VP. Micellar nanocarriers: Pharmaceutical perspectives. Pharm. Res. 2007; 24(1):1–16. [PubMed: 17109211]
4. Cuenca AG, Jiang H, Hochwald SN, Delano M, Cance WG, Grobmyer SR. Emerging implications of nanotechnology on cancer diagnostics and therapeutics. Cancer. 2006; 107(3):459–466. [PubMed: 16795065]
5. Grobmyer, SR.; Moudgil, BM., editors. Methods in Molecular Biology. Vol. Vol. 624. Totowa: Humana Press Inc; 2011. Cancer Nanotechnology: Methods and Protocols.
6. Bao A, Goins B, Klipper R, Negrete G, Phillips WT. Direct $^{99m}$Tc labeling of PEGylated liposomal doxorubicin (Doxil) for pharmacokinetic and non-invasive imaging studies. J. Pharmacol. Exp. Ther. 2004; 308(2):419–425. [PubMed: 14610219]
7. Chuang K-H, et al. Endocytosis of PEGylated agents enhances cancer imaging and anticancer efficacy. Mol. Cancer Ther. 2010; 9(6):1903–1912. [PubMed: 20501805]
8. Barenholz Y. Doxil® - The first FDA-approved nano-drug: Lessons learned. J. Control. Release. 2012; 160(2):117–134. [PubMed: 22484195]
9. Green MR, Manikhas GM, Orlov S, Afanasyev B, Makhson AM, Bhar P, Hawkins MJ. Abraxane®, a novel Cremophor®-free, albumin-bound particle form of paclitaxel for the treatment of advanced non-small-cell lung cancer. Ann. Oncol. 2006; 17(8):1263–1268. [PubMed: 16740598]
10. It should be noted that nanoscale formulations do not always result in nanoscale drug delivery; for instance, the nanoparticles in Abraxane® readily dissociate into individual drug-bound albumin species after injection. See: Desai N. Nab technology: A drug delivery platform utilizing endothelial gp60 receptor-based transport and tumour-derived SPARC for targeting. Drug Delivery Report (16th ed). 2007:37–41.
11. Deitcher OR, O'Brien S, Deitcher SR, Thomas DA, Kantarjian HM. Single-agent vincristine sulfate liposomes injection (Marqibo®) compared to historical single-agent therapy for adults with advanced, relapsed and/or refractory Philadelphia chromosome negative acute lymphoblastic leukemia. Blood. 2011; 118(21):1112–1113.
12. Duncan R, Gaspar R. Nanomedicine(s) under the Microscope. Mol. Pharm. 2011; 8(6):2101–2141. [PubMed: 21974749]
13. Wang AZ, Langer R, Farokhzad OC. Nanoparticle delivery of cancer drugs. Annu. Rev. Med. 2012; 63(1):185–198. [PubMed: 21888516]
14. Lammers T, Kiessling F, Hennink WE, Storm G. Drug targeting to tumors: Principles, pitfalls and (pre-) clinical progress. J. Control. Release. 2012; 161(2):175–187. [PubMed: 21945285]
15. Petre CE, Dittmer DP. Liposomal daunorubicin as treatment for Kaposi's sarcoma. Int. J. Nanomed. 2007; 2(3):277–288.

16. Wang Y-XJ. Superparamagnetic iron oxide based MRI contrast agents: Current status of clinical application. Quant. Imaging Med. Surg. 2011; 1(1):35–40.
17. Goodwill, P.; Krishnan, KM.; Conolly, SM. Magnetic nanoparticles: from fabrication to clinical applications. Thanh, NTK., editor. Boca Raton: CRC Press; 2012. p. 523-440.
18. Maier-Hauff K, Ulrich F, Nestler D, Niehoff H, Wust P, Thiesen B, Orawa H, Budach V, Jordan A. Efficacy and safety of intratumoral thermotherapy using magnetic iron-oxide nanoparticles combined with external beam radiotherapy on patients with recurrent glioblastoma multiforme. J. Neuro-Oncol. 2011; 103(2):317–324.
19. Feng ZL, Zhao G, Yu L, Gough D, Howell SB. Preclinical efficacy studies of a novel nanoparticle-based formulation of paclitaxel that out-performs Abraxane. Cancer Chemother. Pharmacol. 2010; 65(5):923–930. [PubMed: 19685054]
20. Von Hoff DD, Jameson G, Borad MJ, Rosen LS, Utz J, Dhar S, Acosta L, Barker T, Walling J, Hamm JT. First Phase I trial of NKTR-102 (PEG-irinotecan) reveals early evidence of broad anti-tumor activity in three schedules. EJC Suppl. 2008; 6(12):186. 20th EORTC-NCI-AACR Mol. Symp. Mol.Targets & Cancer Therapeutics, Poster #595.
21. Landon CD, Park J-Y, Needham D, Dewhirst MW. Nanoscale drug delivery and hyperthermia: The materials design and preclinical and clinical testing of low temperature-sensitive liposomes used in combination with mild hyperthermia in the treatment of local cancer. Open Nanomed. J. 2011; 3:38–64.
22. Kim D-W, Kim S-Y, Kim H-K, Kim S-W, Shin SW, Kim JS, Park K, Lee MY, Heo DS. Multicenter phase II trial of Genexol-PM, a novel Cremophor-free, polymeric micelle formulation of paclitaxel, with cisplatin in patients with advanced non-small-cell lung cancer. Ann. Oncol. 2007; 18(12):2009–2014. [PubMed: 17785767]
23. Saif MW, Podoltsev NA, Rubin MS, Figueroa JA, Lee MY, Kwon J, Rowen E, Yu J, Kerr RO. Phase II clinical trial of paclitaxel loaded polymeric micelle in patients with advanced pancreatic cancer. Cancer Invest. 2011; 28(2):186–194. [PubMed: 19968498]
24. Dicko A, Kwak S, Frazier AA, Mayer LD, Liboiron BD. Biophysical characterization of a liposomal formulation of cytarabine and daunorubicin. Int. J. Pharm. 2010; 391(1–2):248–259. [PubMed: 20156541]
25. Feldman EJ, Kolitz JE, Trang JM, Liboiron BD, Swenson CE, Chiarella MT, Mayer LD, Louie AC, Lancet JE. Pharmacokinetics of CPX-351; a nano-scale liposomal fixed molar ratio formulation of cytarabine:daunorubicin, in patients with advanced leukemia. Leukemia Res. 2012; 36(10):1283–1289. [PubMed: 22840315]
26. Gordon EM, Hall FL. Rexin-G, a targeted genetic medicine for cancer. Expert Opin.Biol. Ther. 2010; 10(5):819–832. [PubMed: 20384524]
27. Davis ME. Design and development of IT-101, a cyclodextrin-containing polymer conjugate of camptothecin. Adv. Drug Deliv. Rev. 2009; 61(13):1189–1192. [PubMed: 19682514]
28. Walsh MD, Hanna SK, Sen J, Rawal S, Cabral CB, Yurkovetskiy AV, Fram RJ, Lowinger TB, Zamboni WC. Pharmacokinetics and antitumor efficacy of XMT-1001, a novel, polymeric topoisomerase I inhibitor, in mice bearing HT-29 human colon carcinoma xenografts. Clin. Cancer Res. 2012; 18(9):2591–2602. [PubMed: 22392910]
29. Davis ME. The first targeted delivery of siRNA in humans via a self-assembling, cyclodextrin polymer-based nanoparticle: From concept to clinic. Mol. Pharm. 2009; 6(3):659–668. [PubMed: 19267452]
30. Davis ME, Zuckerman JE, Choi CHJ, Seligson D, Tolcher A, Alabi CA, Yen Y, Heidel JD, Ribas A. Evidence of RNAi in humans from systemically administered siRNA via targeted nanoparticles. Nature. 2010; 464(7291):1067–1070. [PubMed: 20305636]
31. Shi J, Xiao Z, Kamaly N, Farokhzad OC. Self-assembled targeted nanoparticles: Evolution of technologies and bench to bedside translation. Acc. Chem. Res. 2011; 44(10):1123–1134. [PubMed: 21692448]
32. Hrkach J, von Hoff D, Ali MM, Andrianova E, Auer J, Campbell T, De Witt D, Figa M, Figueiredo M, Horhota A, Low S, McDonnell K, Peeke E, Retnarajan B, Sabnis A, Schnipper E, Song JJ, Song YH, Summa J, Tompsett D, Troiano G, Van geen Hoven T, Wright J, LoRusso P, Kantoff PW, Bander NH, Sweeney C, Farokhzad OC, Langer R, Zale S. Preclinical development

and clinical translation of a PSMA-targeted docetaxel nanoparticle with a differentiated pharmacological profile. Sci. Transl. Med. 2012; 4:128ra139.

33. Libutti SK, Paciotti GF, Byrnes AA, Alexander HR, Gannon WE, Walker M, Seidel GD, Yuldasheva N, Tamarkin L. Phase I and pharmacokinetic studies of CYT-6091, a novel PEGylated colloidal gold-rhTNF nanomedicine. Clin. Cancer Res. 2010; 16(24):6139–6149. [PubMed: 20876255]
34. Jain MM, Deshmukh CD, Bhatt NN, Bondarde SA, Nagarkar RV, Divekar CJDGH. Phase I, PK, dose-finding, active controlled study of paclitaxel injection concentrate for nanodispersion (PICN) in subjects with metastatic breast cancer. J. Clin. Oncol. 2011; 29(Suppl.) abstr. e11585.
35. Levy L, Herrera A, Devauchelle P, Bonvalot S, Deutsch E, Le Pechoux C. NBTXR3 nanoparticles for radioenhancement: Rationle for the first-in-man study in advanced soft tissue sarcoma. Ann. Oncol. 2012; 23(Suppl. 1):17–18.
36. Lal S, Clare SE, Halas NJ. Nanoshell-enabled photothermal cancer therapy: Impending clinical impact. Acc. Chem. Res. 2008; 41(12):1842–1851. [PubMed: 19053240]
37. Benezra M, Penate-Medina O, Zanzonico PB, Schaer D, Ow H, Burns A, DeStanchina E, Longo V, Herz E, Iyer S, Wolchok J, Larson SM, Wiesner U, Bradbury MS. Multimodal silica nanoparticles are effective cancer-targeted probes in a model of human melanoma. J. Clin. Invest. 2011; 121(7):2768–2780. [PubMed: 21670497]
38. Jain RK, Stylianopoulos T. Delivering nanomedicine to solid tumors. Nat. Rev. Clin. Oncol. 2010; 7(11):653–664. [PubMed: 20838415]
39. Smith BR, Kempen P, Bouley D, Xu A, Liu Z, Melosh N, Dai H, Sinclair R, Gambhir SS. Shape matters: Intravital microscopy reveals surprising geometrical dependence for nanoparticles in tumor models of extravasation. Nano Lett. 2012; 12(7):3369–3377. [PubMed: 22650417]
40. Chithrani BD, Ghazani AA, Chan WCW. Determining the size and shape dependence of gold nanoparticle uptake into mammalian cells. Nano Lett. 2006; 6(4):662–668. [PubMed: 16608261]
41. Jiang W, Kim BYS, Rutka JT, Chan WCW. Nanoparticle-mediated cellular response is size-dependent. Nature Nanotech. 2008; 3(3):145–150.
42. Maeda H. Tumor-Selective Delivery of macromolecular drugs via the EPR Effect: Background and future prospects. Bioconjug. Chem. 2010; 21(5):797–802. [PubMed: 20397686]
43. Perrault SD, Walkey C, Jennings T, Fischer HC, Chan WCW. Mediating tumor targeting efficiency of nanoparticles through design. Nano Lett. 2009; 9(5):1909–1915. [PubMed: 19344179]
44. Dreher MR, Liu W, Michelich CR, Dewhirst MW, Yuan F, Chilkoti A. Tumor vascular permeability, accumulation, and penetration of macromolecular drug carriers. J. Natl. Cancer Inst. 2006; 98(5):335–344. [PubMed: 16507830]
45. Sarin H, Kanevsky AS, Wu HT, Sousa AA, Wilson CM, Aronova MA, Griffiths GL, Leapman RD, Vo HQ. Physiologic upper limit of pore size in the blood-tumor barrier of malignant solid tumors. J. Transl. Med. 2009; 7:51. (13 pages). [PubMed: 19549317]
46. Chauhan VP, Stylianopoulos T, Martin JD, Popovic Z, Chen O, Kamoun WS, Bawendi MG, Fukumura D, Jain RK. Normalization of tumour blood vessels improves the delivery of nanomedicines in a size-dependent manner. Nature Nanotech. 2012; 7(6):383–388.
47. Khlebtsov N, Dykman L. Biodistribution and toxicity of engineered gold nanoparticles: a review of in vitro and in vivo studies. Chem. Soc. Rev. 2012; 40(3):1647–1671. [PubMed: 21082078]
48. Park J, Lim D-H, Lim H-J, Kwon T, Choi J-s, Jeong S, Choi I-H, Cheon J. Size dependent macrophage responses and toxicological effects of Ag nanoparticles. Chem. Commun. 2011; 47(15):4382–4384.
49. Xia W, Song H-M, Wei Q, Wei A. Differential response of macrophages to core-shell $Fe_3O_4$@Au nanoparticles and nanostars. Nanoscale. 2012; 4(22):7143–7148. [PubMed: 23069807]
50. Kobayashi H, Brechbiel MW. Dendrimer-based macromolecular MRI contrast agents: Characteristics and application. Mol. Imaging. 2003; 2(1):1–10. [PubMed: 12926232]
51. Choi HS, Liu W, Misra P, Tanaka E, Zimmer JP, Itty Ipe B, Bawendi MG, Frangioni JV. Renal clearance of quantum dots. Nat. Biotechnol. 2007; 25(10):1165–1170. [PubMed: 17891134]

52. Fox ME, Szoka FC, Fréchet JMJ. Soluble polymer carriers for the treatment of cancer: The importance of molecular architecture. Acc. Chem. Res. 2009; 42(8):1141–1151. [PubMed: 19555070]
53. Xu S, Nie Z, Seo M, Lewis P, Kumacheva E, Stone HA, Garstecki P, Weibel DB, Gitlin I, Whitesides GM. Generation of monodisperse particles by using microfluidics: Control over size, shape, and composition. Angew. Chem. Int. Ed. 2005; 44(25):3799–3799.
54. Berne, BJ.; Pecora, R. Dynamic light scattering: with applications to chemistry, biology, and physics. Mineola, N.Y.: Dover Publications; 2000.
55. Philo JS. A critical review of methods for size characterization of non-particulate protein aggregates. Curr. Pharm. Biotechnol. 2009; 10(4):359–372. [PubMed: 19519411]
56. Fraunhofer W, Winter G, Coester C. Asymmetrical flow field-flow fractionation and multiangle light scattering for analysis of gelatin nanoparticle drug carrier systems. Anal. Chem. 2004; 76(7): 1909–1920. [PubMed: 15053651]
57. Bootz A, Vogel V, Schubert D, Kreuter J. Comparison of scanning electron microscopy, dynamic light scattering and analytical ultracentrifugation for the sizing of poly(butyl cyanoacrylate) nanoparticles. Eur. J. Pharm. Biopharm. 2004; 57(2):369–375. [PubMed: 15018998]
58. Liu J, Andya J, Shire S. A critical review of analytical ultracentrifugation and field flow fractionation methods for measuring protein aggregation. AAPS J. 2006; 8(3):E580–E589. [PubMed: 17025276]
59. Zook JM, Rastogi V, MacCuspie RI, Keene AM, Fagan J. Measuring agglomerate size distribution and dependence of localized surface plasmon resonance absorbance on gold nanoparticle agglomerate size using analytical ultracentrifugation. ACS Nano. 2011; 5(10):8070–8079. [PubMed: 21888410]
60. Luo, Y.; Matejic, T.; Ng, C-K.; Nunnally, B.; Porter, T.; Raso, S.; Rouse, J.; Shang, T.; Steckert, J.; Satinder, A.; Stephen, S. In Separation Science and Technology. Vol. Vol. 10. Academic Press; 2011. p. 283-359.
61. Huo Q. Protein complexes/aggregates as potential cancer biomarkers revealed by a nanoparticle aggregation immunoassay. Colloid Surf. B. 2010; 78(2):259–265.
62. Dai Q, Liu X, Coutts J, Austin L, Huo Q. A one-step highly sensitive method for DNA detection using dynamic light scattering. J. Am. Chem. Soc. 2008; 130(26):8138–8139. [PubMed: 18540598]
63. Vogel R, Willmott G, Kozak D, Roberts GS, Anderson W, Groenewegen L, Glossop B, Barnett A, Turner A, Trau M. Quantitative sizing of nano/microparticles with a tunable elastomeric pore sensor. Anal. Chem. 2011; 83(9):3499–3506. [PubMed: 21434639]
64. Roberts GS, Kozak D, Anderson W, Broom MF, Vogel R, Trau M. Tunable nano/micropores for particle detection and discrimination: Scanning ion occlusion spectroscopy. Small. 2010; 6(23): 2653–2658. [PubMed: 20979105]
65. Montes-Burgos I, Walczyk D, Hole P, Smith J, Lynch I, Dawson K. Characterisation of nanoparticle size and state prior to nanotoxicological studies. J. Nanoparticle Res. 2010; 12(1):47–53.
66. Filipe V, Hawe A, Jiskoot W. Critical evaluation of nanoparticle tracking analysis (nta) by nanosight for the measurement of nanoparticles and protein aggregates. Pharm. Res. 2010; 27(5): 796–810. [PubMed: 20204471]
67. Bell NC, Minelli C, Tompkins J, Stevens MM, Shard AG. Emerging techniques for submicrometer particle sizing applied to Stöber silica. Langmuir. 2012; 28(29):10860–10872. [PubMed: 22724385]
68. Krishnan RS, Sivarajan SR. Scattering of polarised light by colloids containing anisotropic particles. Proc. Ind. Acad. Sci. 1956; 44(5):274–278. Sec. A.
69. Schwarcz HP, Shane KC. Measurement of particle shape by Fourier analysis. Sedimentology. 1969; 13(3–4):213–231.
70. Loren N, Hamberg L, Hermansson AM. Measuring shapes for application in complex food structures. Food Hydrocolloids. 2006; 20(5):712–722.
71. Petoukhov MV, Svergun DI. Analysis of X-ray and neutron scattering from biomacromolecular solutions. Curr. Op. Struct. Biol. 2007; 17(5):562–571.

72. Reddy NK, Pérez-Juste J, Pastoriza-Santos I, Lang PR, Dhont JKG, Liz-Marzán LM, Vermant J. Flow dichroism as a reliable method to measure the hydrodynamic aspect ratio of gold nanoparticles. ACS Nano. 2011; 5(6):4935–4944. [PubMed: 21545088]
73. Barenholz, Y. Amphipathic weak base loading into preformed liposomes having a transmembrane ammonium ion gradient: From the bench to approved DOXIL. In: Gregoriadis, G., editor. Liposome Technology: Entrapment of Drugs and Other Materials into Liposomes. 3rd ed.. Vol. vol. 2. New York: Informa Healthcare; 2007. p. 1-25.
74. Park J, An K, Hwang Y, Park J-G, Noh H-J, Kim J-Y, Park J-H, Hwang N-M, Hyeon T. Ultra-large-scale syntheses of monodisperse nanocrystals. Nature Mater. 2004; 3(12):891–895. [PubMed: 15568032]
75. Xia Y, Xiong Y, Lim B, Sara E Skrabalak. Shape-controlled synthesis of metal nanocrystals: Simple chemistry meets complex physics? Angew. Chem. Int. Ed. 2009; 48(1):60–103.
76. Park JI, Saffari A, Kumar S, Günther A, Kumacheva E. Microfluidic synthesis of polymer and inorganic particulate materials. Annu. Rev. Mater. Res. 2010; 40(1):415–443.
77. Drobot M. Continuous flow microreactors in nanoparticle synthesis. Spec. Chem. Mag. 2012; 32(5):40–41.
78. Jin HD, Garrison A, Tseng T, Paul BK, Chang C-H. High-rate synthesis of phosphine-stabilized undecagold nanoclusters using a multilayered micromixer. Nanotechnology. 2010; 21(44):445604. [PubMed: 20935355]
79. Wagner J, Köhler JM. Continuous synthesis of gold nanoparticles in a microreactor. Nano Lett. 2005; 5(4):685–691. [PubMed: 15826109]
80. Hartlieb KJ, Raston CL, Saunders M. Controlled scalable synthesis of ZnO nanoparticles. Chem. Mater. 2007; 19(23):5453–5459.
81. Marre S, Jensen KF. Synthesis of micro and nanostructures in microfluidic systems. Chem. Soc. Rev. 2010; 39(3):1183–1202. [PubMed: 20179831]
82. Capretto L, Mazzitelli S, Brognara E, Lampronti I, Carugo D, Hill M, Zhang X, Gambari R, Nastruzzi C. Mithramycin encapsulated in polymeric micelles by microfluidic technology as novel therapeutic protocol for beta-thalassemia. Int. J. Nanomed. 2012; 7(1):307–324.
83. Loh JW, Schneider J, Carter M, Saunders M, Lim LY. Spinning disc processing technology: Potential for large-scale manufacture of chitosan nanoparticles. J. Pharm. Sci. 2010; 99(10):4326–4336. [PubMed: 20737637]
84. Perry JL, Herlihy KP, Napier ME, DeSimone JM. PRINT: A novel platform toward shape and size specific nanoparticle theranostics. Acc. Chem. Res. 2011; 44(10):990–998. [PubMed: 21809808]
85. Wang Y, Byrne JD, Napier ME, DeSimone JM. Engineering nanomedicines using stimuli-responsive biomaterials. Adv. Drug Deliv. Rev. 2012; 64(11):1021–1030. [PubMed: 22266128]
86. Wang J-T, Wang J, Han J-J. Fabrication of advanced particles and particle-based materials assisted by droplet-based microfluidics. Small. 2011; 7(13):1728–1754. [PubMed: 21618428]
87. Li S-D, Huang L. Pharmacokinetics and biodistribution of nanoparticles. Mol. Pharm. 2008; 5(4): 496–504. [PubMed: 18611037]
88. Dobrovolskaia MA, McNeil SE. Immunological properties of engineered nanomaterials. Nature Nanotech. 2007; 2(8):469–478.
89. Poulin P, Haddad S. Advancing prediction of tissue distribution and volume of distribution of highly lipophilic compounds from a simplified tissue-composition-based model as a mechanistic animal alternative method. J. Pharm. Sci. 2012; 101(6):2250–2261. [PubMed: 22388869]
90. Rostami-Hodjegan A. Physiologically based pharmacokinetics joined with in vitro-in vivo extrapolation of ADME: A marriage under the arch of systems pharmacology. Clin. Pharmacol. Ther. 2012; 92(1):50–61. [PubMed: 22644330]
91. Landsiedel R, Fabian E, Ma-Hock L, Wohlleben W, Wiench K, Oesch F, van Ravenzwaay B. Toxico-/biokinetics of nanomaterials. Arch. Toxicol. 2012; 86(7):1021–1060. [PubMed: 22576463]
92. Tucker GT. An agenda for UK clinical pharmacology: Research priorities in pharmacokinetics. Br. J. Clin. Pharmacol. 2012; 73(6):924–926. [PubMed: 22360418]
93. Walters WP. Going further than Lipinski's rule in drug design. Expert. Opin. Drug Discov. 2012; 7(2):99–107. [PubMed: 22468912]

94. Hussain S, Vanoirbeek JAJ, Hoet PHM. Interactions of nanomaterials with the immune system. WIREs – Nanomed. Nanobiotechnol. 2011; 4(2):169–183.

95. Bartneck M, Keul HA, Singh S, Czaja K, Bornemann J, Bockstaller M, Moeller M, Zwadlo-Klarwasser G, Groll J. Rapid uptake of gold nanorods by primary human blood phagocytes and immunomodulatory effects of surface chemistry. ACS Nano. 2010; 4(6):3073–3086. [PubMed: 20507158]

96. Zhang XD, Wu D, Shen X, Liu PX, Yang N, Zhao B, Zhang H, Sun YM, Zhang LA, Fan FY. Size-dependent *in vivo* toxicity of PEG-coated gold nanoparticles. Int. J. Nanomed. 2011; 6:2071–2081.

97. Cho W-S, Cho M, Jeong J, Choi M, Cho H-Y, Han BS, Kim SH, Kim HO, Lim YT, Chung BH, Jeong J. Acute toxicity and pharmacokinetics of 13 nm-sized PEG-coated gold nanoparticles. Toxicol. Appl. Pharmacol. 2009; 236(1):16–24. [PubMed: 19162059]

98. Huff TB, Hansen MN, Zhao Y, Cheng J-X, Wei A. Controlling the cellular uptake of gold nanorods. Langmuir. 2007; 23(4):1596–1599. [PubMed: 17279633]

99. Leonov AP, Zheng J, Clogston JD, Stern ST, Patri AK, Wei A. Detoxification of gold nanorods by treatment with polystyrenesulfonate. ACS Nano. 2008; 2(12):2481–2488. [PubMed: 19206282]

100. Murphy CJ, Gole AM, Stone JW, Sisco PN, Alkilany AM, Goldsmith EC, Baxter SC. Gold nanoparticles in biology: Beyond toxicity to cellular imaging. Acc. Chem. Res. 2008; 41(12): 1721–1730. [PubMed: 18712884]

101. Wei, A.; Leonov, AP.; Wei, QS. Gold nanorods: Multifunctional agents for cancer imaging and therapy. In: Grobmyer, SR.; Moudgil, BM., editors. Cancer Nanotechnology: Methods and Protocols. Vol. Vol. 624. Totowa: Humana Press Inc; 2011. p. 119-130.

102. Kumagai M, Sarma TK, Cabral H, Kaida S, Sekino M, Herlambang N, Osada K, Kano MR, Nishiyama N, Kataoka K. Enhanced *in vivo* magnetic resonance imaging of tumors by PEGylated iron-oxide–gold core–shell nanoparticles with prolonged blood circulation properties. Macromol. Rapid Commun. 2010; 31(17):1521–1528. [PubMed: 21567561]

103. Prencipe G, Tabakman SM, Welsher K, Liu Z, Goodwin AP, Zhang L, Henry J, Dai HJ. PEG branched polymer for functionalization of nanomaterials with ultralong blood circulation. J. Am. Chem. Soc. 2009; 131(13):4783–4787. [PubMed: 19173646]

104. Tong L, He W, Zhang Y, Zheng W, Cheng J-X. Visualizing systemic clearance and cellular level biodistribution of gold nanorods by intrinsic two-photon luminescence. Langmuir. 2009; 25(21): 12454–12459. [PubMed: 19856987]

105. Lankveld DPK, Rayavarapu RG, Krystek P, Oomen AG, Verharen HW, van Leeuwen TG, De Jong WH, Manohar S. Blood clearance and tissue distribution of PEGylated and non-PEGylated gold nanorods after intravenous administration in rats. Nanomedicine. 2011; 6(2):339–349. [PubMed: 21385136]

106. Akiyama Y, Mori T, Katayama Y, Niidome T. The effects of PEG grafting level and injection dose on gold nanorod biodistribution in the tumor-bearing mice. J. Control. Release. 2009; 139(1):81–84. [PubMed: 19538994]

107. von Maltzahn G, Park J-H, Agrawal A, Bandaru NK, Das SK, Sailor MJ, Bhatia SN. Computationally guided photothermal tumor therapy using long-circulating gold nanorod antennas. Cancer Res. 2009; 69(9):3892–3900. [PubMed: 19366797]

108. Goodrich GP, Bao LL, Gill-Sharp K, Sang KL, Wang J, Payne JD. Photothermal therapy in a murine colon cancer model using near-infrared absorbing gold nanorods. J. Biomed. Opt. 2010; 15(1):018001. [PubMed: 20210487]

109. Zhang G, Yang Z, Lu W, Zhang R, Huang Q, Tian M, Li L, Liang D, Li C. Influence of anchoring ligands and particle size on the colloidal stability and *in vivo* biodistribution of polyethylene glycol-coated gold nanoparticles in tumor-xenografted mice. Biomaterials. 2009; 30(10):1928–1936. [PubMed: 19131103]

110. Malmsten M, Emoto K, Van Alstine JM. Effect of chain density on inhibition of protein adsorption by poly(ethylene glycol) based coatings. J. Colloid Interface Sci. 1998; 202(2):507–517.

111. Unsworth LD, Sheardown H, Brash JL. Protein-resistant poly(ethylene oxide)-grafted surfaces: Chain density-dependent multiple mechanisms of action. Langmuir. 2008; 24(5):1924–1929. [PubMed: 18217777]

112. Ngadi N, Abrahamson J, Fee C, Morison K. Are PEG molecules a universal protein repellent? World Acad. Sci. Eng. Technol. 2009; 49:144–148.

113. Cheng T-L, Chuang K-H, Chen B-M, Roffler SR. Analytical measurement of PEGylated molecules. Bioconjug. Chem. 2012; 23(5):881–899.

114. Otsuka H, Nagasaki Y, Kataoka K. PEGylated nanoparticles for biological and pharmaceutical applications. Adv. Drug Deliv. Rev. 2003; 55(3):403–419. [PubMed: 12628324]

115. Karakoti AS, Das S, Thevuthasan S, Seal S. PEGylated inorganic nanoparticles. Angew. Chem. Int. Ed. 2011; 50(9):1980–1994.

116. Efremova NV, Sheth SR, Leckband DE. Protein-induced changes in poly(ethylene glycol) brushes: Molecular weight and temperature dependence. Langmuir. 2001; 17(24):7628–7636.

117. Heuberger M, Drobek T, Spencer ND. Interaction forces and morphology of a protein-resistant poly(ethylene glycol) layer. Biophys. J. 2005; 88(1):495–504. [PubMed: 15501935]

118. Klibanov AL, Maruyama K, Beckerleg AM, Torchilin VP, Huang L. Activity of amphipathic poly(ethylene glycol) 5000 to prolong the circulation time of liposomes depends on the liposome size and is unfavorable for immunoliposome binding to target. Biochim Biophys. Acta – Biomembranes. 1991; 1062(2):142–148.

119. Allen TM. Ligand-targeted therapeutics in anticancer therapy. Nature Rev. Cancer. 2002; 2(10): 750–763. [PubMed: 12360278]

120. Hak S, Helgesen E, Hektoen HH, Huuse EM, Jarzyna PA, Mulder WJM, Haraldseth O, Davies CDL. The effect of nanoparticle polyethylene glycol surface density on ligand-directed tumor targeting studied *in vivo* by dual modality imaging. ACS Nano. 2012; 6(6):5648–5658. [PubMed: 22671719]

121. Huang X, Peng X, Wang Y, Wang Y, Shin DM, El-Sayed MA, Nie S. A reexamination of active and passive tumor targeting by using rod-shaped gold nanocrystals and covalently conjugated peptide ligands. ACS Nano. 2010; 4(10):5887–5896. [PubMed: 20863096]

122. Sarin H. Overcoming the challenges in the effective delivery of chemotherapies to CNS solid tumors. Ther. Deliv. 2010; 1(2):289–305. [PubMed: 22163071]

123. Patri AK. unpublished results.

124. Xia W, Low PS. Folate-targeted therapies for cancer. J. Med. Chem. 2010; 53(19):6811–6824. [PubMed: 20666486]

125. Huff TB, Tong L, Zhao Y, Hansen MN, Cheng J-X, Wei A. Hyperthermic effects of gold nanorods on tumor cells. Nanomedicine. 2007; 2(1):125–132. [PubMed: 17716198]

126. Swanson SD, Kukowska-Latallo JF, Patri AK, Chen CY, Ge S, Cao ZY, Kotlyar A, East AT, Baker JR. Targeted gadolinium-loaded dendrimer nanoparticles for tumor-specific magnetic resonance contrast enhancement. Int. J. Nanomed. 2008; 3(2):201–210.

127. Pons T, Medintz IL, Wang X, English DS, Mattoussi H. Solution-phase single quantum dot fluorescence resonance energy transfer. J. Am. Chem. Soc. 2006; 128(47):15324–15331. [PubMed: 17117885]

128. Demers LM, Mirkin CA, Mucic RC, Reynolds RA III, Letsinger RL, Elghanian R, Viswanadham G. A fluorescence-based method for determining the surface coverage and hybridization efficiency of thiol-capped oligonucleotides bound to gold thin films and nanoparticles. Anal. Chem. 2000; 72(22):5535–5541. [PubMed: 11101228]

129. Maus L, Spatz JP, Fiammengo R. Quantification and reactivity of functional groups in the ligand shell of PEGylated gold nanoparticles via a fluorescence-based assay. Langmuir. 2009; 25(14): 7910–7917. [PubMed: 19419188]

130. Wang X, Ramstrom O, Yan M. A photochemically initiated chemistry for coupling underivatized carbohydrates to gold nanoparticles. J. Mater. Chem. 2009; 19(47):8944–8949. [PubMed: 20856694]

131. Wang X, Ramström O, Yan M. Quantitative analysis of multivalent ligand presentation on gold glyconanoparticles and the impact on lectin binding. Anal. Chem. 2011; 82(21):9082–9089.

132. He W, Henne WA, Wei Q, Zhao Y, Doorneweerd DD, Cheng J-X, Low PS, Wei A. Two-photon luminescence imaging of *Bacillus* spores using peptide-functionalized gold nanorods. Nano Res. 2008; 1(6):450–456. [PubMed: 20098661]

133. Harkness KM, Hixson BC, Fenn LS, Turner BN, Rape AC, Simpson CA, Huffman BJ, Okoli TC, McLean JA, Cliffel DE. A structural mass spectrometry strategy for the relative quantitation of ligands on mixed monolayer-protected gold nanoparticles. Anal. Chem. 2010; 82(22):9268–9274. [PubMed: 20968282]

134. Elzey S, Tsai D-H, Rabb S, Yu L, Winchester M, Hackley V. Quantification of ligand packing density on gold nanoparticles using ICP-OES. Anal. Bioanal. Chem. 2012; 403(1):145–149. [PubMed: 22349346]

135. Li YL, Gross ML. Ionic-liquid matrices for quantitative analysis by MALDI-TOF mass spectrometry. J. Am. Soc. Mass Spectrom. 2004; 15(12):1833–1837. [PubMed: 15589759]

136. Mrksich M. Mass spectrometry of self-assembled monolayers: A new tool for molecular surface science. ACS Nano. 2008; 2(1):7–18. [PubMed: 19206542]

137. Zhu ZJ, Yeh YC, Tang R, Yan B, Tamayo J, Vachet RW, Rotello VM. Stability of quantum dots in live cells. Nat. Chem. 2011; 3(12):963–968. [PubMed: 22109277]

138. Yan B, Zhu ZJ, Miranda OR, Chompoosor A, Rotello VM, Vachet RW. Laser desorption/ionization mass spectrometry analysis of monolayer-protected gold nanoparticles. Anal. Bioanal. Chem. 2010; 396(3):1025–1035. [PubMed: 19911174]

139. Ju S, Yeo W-S. Quantification of proteins on gold nanoparticles by combining MALDI-TOF MS and proteolysis. Nanotechnology. 2012; 23(13):135701. [PubMed: 22417878]

140. Guha S, Ma X, Tarlov MJ, Zachariah MR. Quantifying ligand adsorption to nanoparticles using tandem differential mobility mass analysis. Anal. Chem. 2012; 84(15):6308–6311. [PubMed: 22769867]

141. Guha S, Li MD, Tarlov MJ, Zechariah MR. Electrospray-differential mobility analysis of bionanoparticles. Trends Biotech. 2012; 30(5):291–300.

142. Kienberger F, Ebner A, Gruber HJ, Hinterdorfer P. Molecular recognition imaging and force spectroscopy of single biomolecules. Acc. Chem. Res. 2005; 39(1):29–36. [PubMed: 16411737]

143. Puchner EM, Gaub HE. Force and function: Probing proteins with AFM-based force spectroscopy. Curr. Op. Struct. Biol. 2009; 19(5):605–614.

144. Bizzarri AR, Cannistraro S. Atomic force spectroscopy in biological complex formation: Strategies and perspectives. J. Phys. Chem. B. 2009; 113(52):16449–16464. [PubMed: 19904973]

145. Li S-D, Huang L. Pharmacokinetics and biodistribution of nanoparticles. Mol. Pharm. 2008; 5(4):496–504. [PubMed: 18611037]

146. Moghimi SM, Hunter AC, Andresen TL. Factors controlling nanoparticle pharmacokinetics: An integrated analysis and perspective. Annu. Rev. Pharmacol. Toxicol. 2012; 52(1):481–503. [PubMed: 22035254]

147. Geng Y, Dalhaimer P, Cai S, Tsai R, Tewari M, Minko T, Discher DE. Shape effects of filaments versus spherical particles in flow and drug delivery. Nat. Nanotech. 2007; 2(4):249–255.

148. Shuvaev VV, Ilies MA, Simone E, Zaitsev S, Kim Y, Cai S, Mahmud A, Dziubla T, Muro S, Discher DE, Muzykantov VR. Endothelial targeting of antibody-decorated polymeric filomicelles. ACS Nano. 2011; 5(9):6991–6999. [PubMed: 21838300]

149. Choi CHJ, Zuckerman JE, Webster P, Davis ME. Targeting kidney mesangium by nanoparticles of defined size. Proc. Natl. Acad. Sci. USA. 2011; 108(16):6656–6661. [PubMed: 21464325]

150. Thakor AS, Jokerst JV, Zavaleta CL, Massoud TF, Gambhir SS. Gold nanoparticles: A revival in precious metal administration to patients. Nano Lett. 2011; 11(10):4029–4036. [PubMed: 21846107]

151. Cheng Y, Meyers JD, Broome A-M, Kenney ME, Basilion JP, Burda C. Deep penetration of a PDT drug into tumors by noncovalent drug-gold nanoparticle conjugates. J. Am. Chem. Soc. 2011; 133(8):2583–2591. [PubMed: 21294543]

152. Cho W-S, Cho M, Jeong J, Choi M, Han BS, Shin H-S, Hong J, Chung BH, Jeong J, Cho M-H. Size-dependent tissue kinetics of PEG-coated gold nanoparticles. Toxicol. Appl. Pharmacol. 2010; 245(1):116–123. [PubMed: 20193702]

153. Chithrani BD, Chan WCW. Elucidating the mechanism of cellular uptake and removal of protein-coated gold nanoparticles of different sizes and shapes. Nano Lett. 2007; 7(6):1542–1550. [PubMed: 17465586]

154. Dreaden EC, Alkilany AM, Huang X, Murphy CJ, El-Sayed MA. The golden age: Gold nanoparticles for biomedicine. Chem. Soc. Rev. 2012; 41(7):2740–2779. [PubMed: 22109657]

155. Dickerson EB, Dreaden EC, Huang X, El-Sayed IH, Chu H, Pushpanketh S, McDonald JF, El-Sayed MA. Gold nanorod assisted near-infrared plasmonic photothermal therapy (PPTT) of squamous cell carcinoma in mice. Cancer Lett. 2008; 269(1):57–66. [PubMed: 18541363]

156. Eghtedari M, Oraevsky A, Copland JA, Kotov N, Conjusteau A, Motamedi M. High sensitivity of *in vivo* detection of gold nanorods using a laser optoacoustic imaging system. Nano Lett. 2007; 7(7):1914–1918. [PubMed: 17570730]

157. Oldenburg AL, Hansen MN, Ralston TS, Wei A, Boppart SA. Imaging gold nanorods in excised human breast carcinoma by spectroscopic optical coherence tomography. J. Mater. Chem. 2009; 19(35):6407–6411. [PubMed: 20107616]

158. Kim C, Song H-M, Cai X, Yao J, Wei A, Wang LV. *In vivo* photoacoustic mapping of lymphatic systems with plasmon-resonant nanostars. J. Mater. Chem. 2011; 21(9):2841–2844. [PubMed: 21660122]

159. Balasubramanian SK, Jittiwat J, Manikandan J, Ong C-N, Yu LE, Ong W-Y. Biodistribution of gold nanoparticles and gene expression changes in the liver and spleen after intravenous administration in rats. Biomaterials. 2010; 31(8):2034–2042. [PubMed: 20044133]

160. Wu G, Mikhailovsky A, Khant HA, Fu C, Chiu W, Zasadzinski JA. Remotely triggered liposome release by near-infrared light absorption via hollow gold nanoshells. J. Am. Chem. Soc. 2008; 130(26):8175–8177. [PubMed: 18543914]

161. Wijaya A, Schaffer SB, Pallares IG, Hamad-Schifferli K. Selective release of multiple DNA oligonucleotides from gold nanorods. ACS Nano. 2009; 3(1):80–86. [PubMed: 19206252]

162. Braun GB, Pallaoro A, Wu G, Missirlis D, Zasadzinski JA, Tirrell M, Reich NO. Laser-activated gene silencing via gold nanoshell-siRNA conjugates. ACS Nano. 2009; 3(7):2007–2015. [PubMed: 19527019]

163. Lu W, Zhang G, Zhang R, Flores LG, Huang Q, Gelovani JG, Li C. Tumor site-specific silencing of NF-kB p65 by targeted hollow gold nanosphere-mediated photothermal transfection. Cancer Res. 2010; 70(8):3177–3188. [PubMed: 20388791]

164. Huschka R, Zuloaga J, Knight MW, Brown LV, Nordlander P, Halas NJ. Light-Induced release of DNA from gold nanoparticles: Nanoshells and nanorods. J. Am. Chem. Soc. 2011; 133(31): 12247–12255. [PubMed: 21736347]

165. Hauck TS, Jennings TL, Yatsenko T, Kumaradas JC, Chan WCW. Enhancing the toxicity of cancer chemotherapeutics with gold nanorod hyperthermia. Adv. Mater. 2008; 20(20):3832–3838.

166. Park H, Yang J, Lee J, Haam S, Choi I-H, Yoo K-H. Multifunctional nanoparticles for combined doxorubicin and photothermal treatments. ACS Nano. 2009; 3(10):2919–2926. [PubMed: 19772302]

167. Huang HC, Yang Y, Nanda A, Koria P, Rege K. Synergistic administration of photothermal therapy and chemotherapy to cancer cells using polypeptide-based degradable plasmonic matrices. Nanomedicine. 2011; 6(3):459–473. [PubMed: 21542685]

168. Hu SH, Liu TY, Liu DM, Chen SY. Nano-ferrosponges for controlled drug release. J. Control. Release. 2007; 121(3):181–189. [PubMed: 17644206]

169. Kong SD, Zhang W, Lee JH, Brammer K, Lal R, Karin M, Jin S. Magnetically vectored nanocapsules for tumor penetration and remotely switchable on-demand drug release. Nano Lett. 2010; 10(12):5088–5092.

170. Thomas CR, Ferris DP, Lee JH, Choi E, Cho MH, Kim ES, Stoddart JF, Shin JS, Cheon J, Zink JI. Noninvasive remote-controlled release of drug molecules in vitro using magnetic actuation of mechanized nanoparticles. J. Am. Chem. Soc. 2010; 132(31):10623–10625. [PubMed: 20681678]

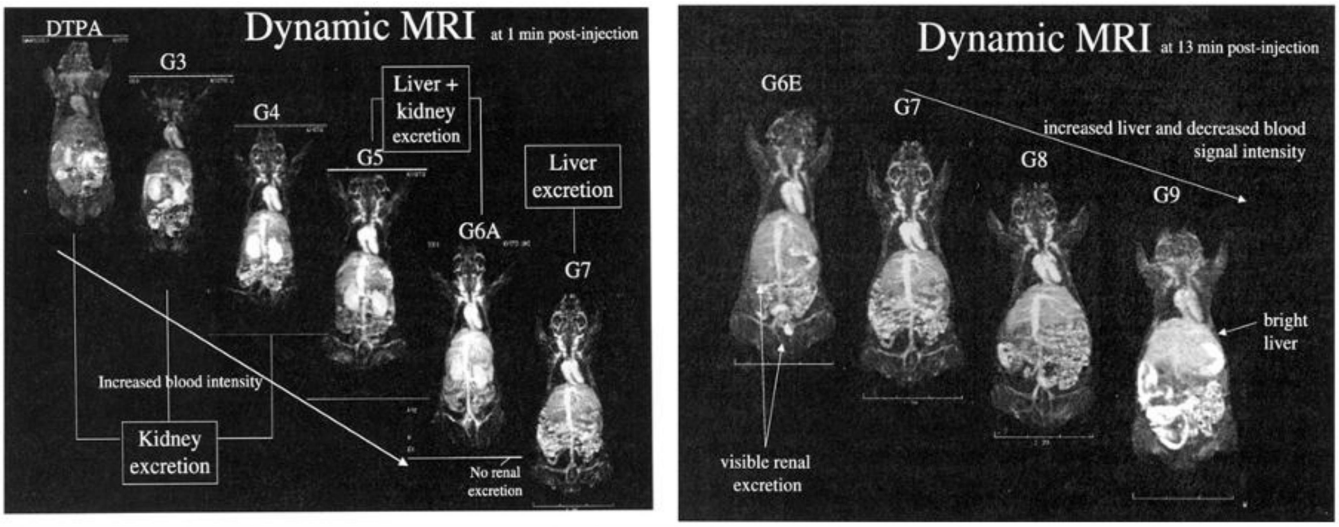


**Fig. 1.**

Elimination of dendrimer-based contrast agents as a function of size (generation), using $T_1$-weighted dynamic MRI. *Left*, coronal image of mice after intravenous administration ($t = 1$ min), with high levels of renal contrast observed for dendrimers up to the 6$^{th}$ generation ($d_h < 10$ nm). *Right*, coronal image of mice inoculated with higher-generation dendrimers ($d_h > 10$ nm, $t = 13$ min) showing increased liver contrast. ©2003 Decker Publishing Inc. (reprinted with permission) [50].

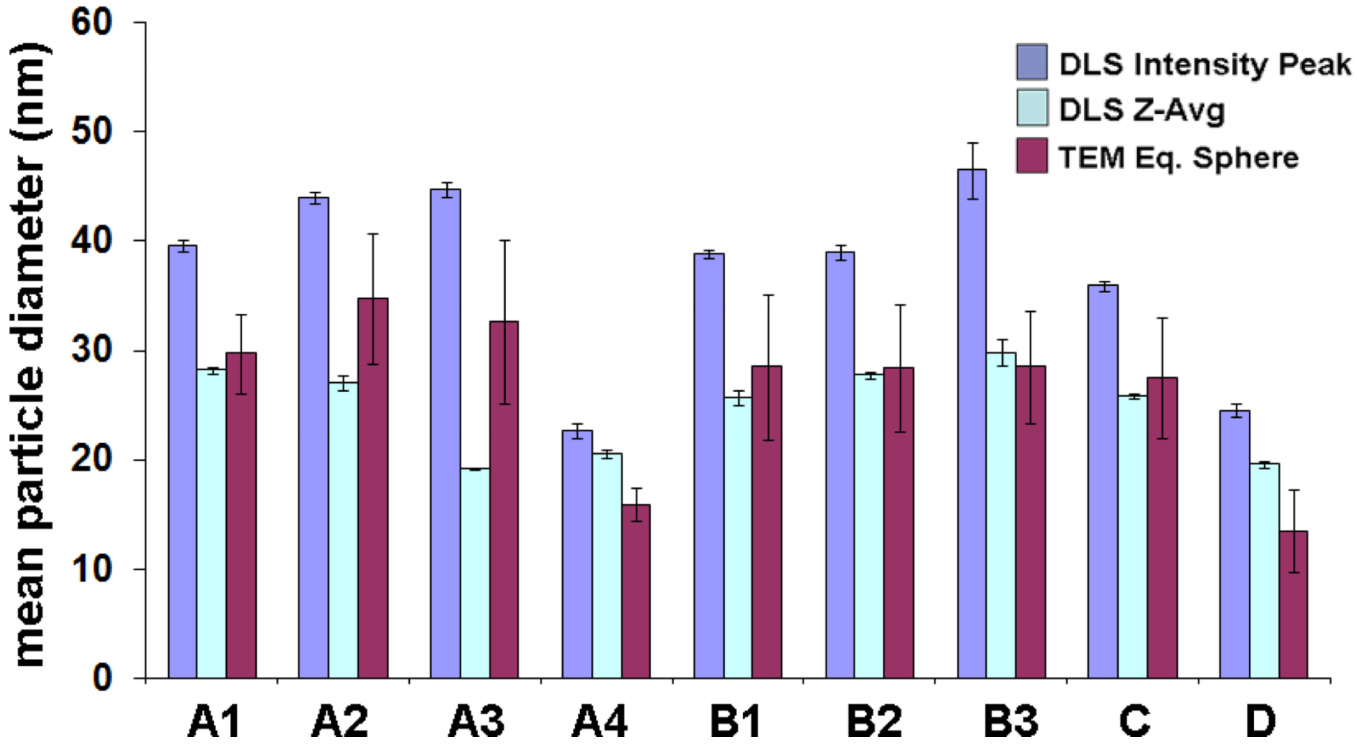


**Fig. 2.**

Comparative analysis of DLS and TEM for size characterization, using citrate-stabilized Au nanoparticles prepared with variations in reaction conditions. In each case, multiple measurements were obtained to establish method accuracy. (A) Na-citrate added to aqueous solution of $HAuCl_4$ at reflux; (B) Na-citrate and $HAuCl_4$ mixed at room temperature, then heated to reflux; (C) $HAuCl_4$ added to Na-citrate solution at reflux; (D) Na-citrate and $HAuCl_4$ added to water at reflux. Note that error bars represent standard deviation of multiple measurements, not size dispersity.

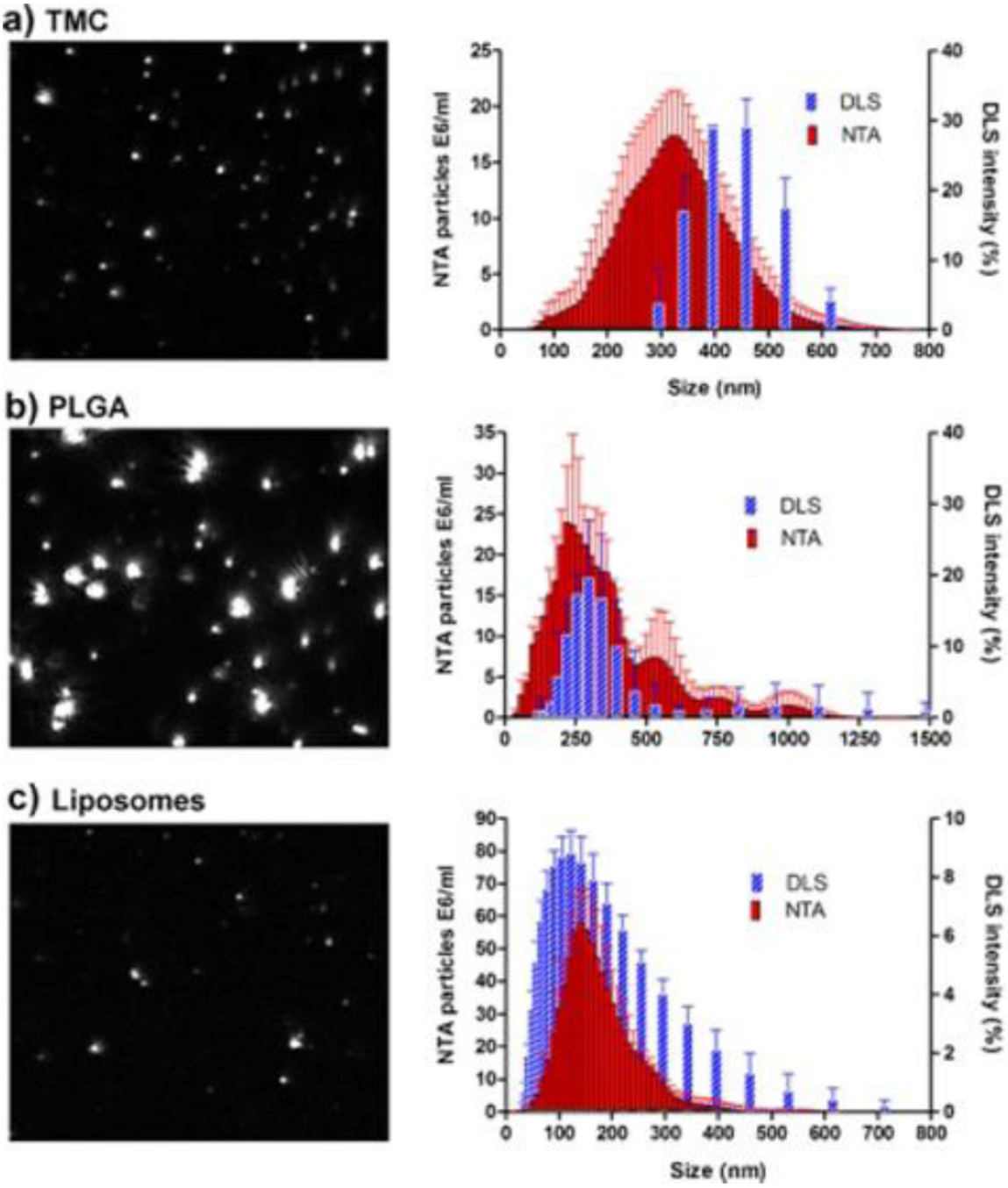


**Fig. 3.**

Size analysis of nanocarriers comprised of (a) trimethyl chitosan (TMC), (b) 50:50 poly(lactic-co-glycolic acid) (PLGA), and (c) commercial liposomes. *Left*, snapshots from NTA video recording; *right*, size distributions by NTA versus DLS, with error bars [66].

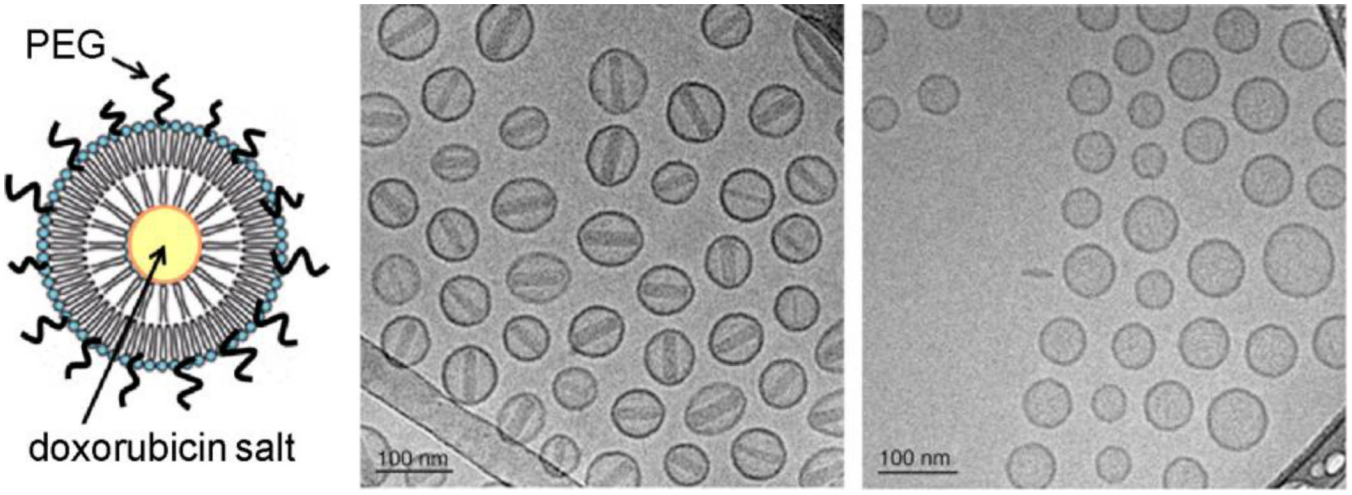


**Fig. 4.**

Cryo-TEM analysis of PEGylated liposomes of (a) doxorubicin sulfate (Doxil®) and (b) doxorubicin glucuronate (Dox-G), prepared by diffusion across a pH gradient [8, 73]. Encapsulated doxorubicin sulfate crystallized into nanorods whereas Dox-G did not, with an apparent impact on pharmacokinetics. © 2012 Elsevier (reprinted with permission) [8].

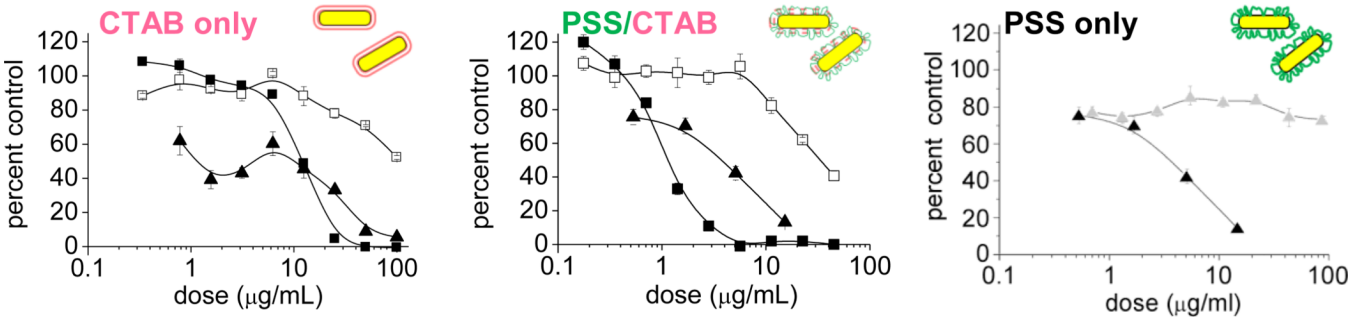


**Fig. 5.**

Cytotoxicity profile of coated Au nanorods (NRs) based on a MTT viability assay, after a 24-h exposure to various cell types: (■) LLC-PK1 cells; (□) HepG2 cells; (▲) KB cells. *Left*, CTAB-stabilized NRs; *middle*, PSS-treated NRs, 11 weeks after purification; (c) *right*, NRs before (▲) and after (Δ) two more rounds of PSS treatment (KB cells only). MTT viability data normalized with respect to a media-only control. © 2008 American Chemical Society (reprinted with permission) [99].

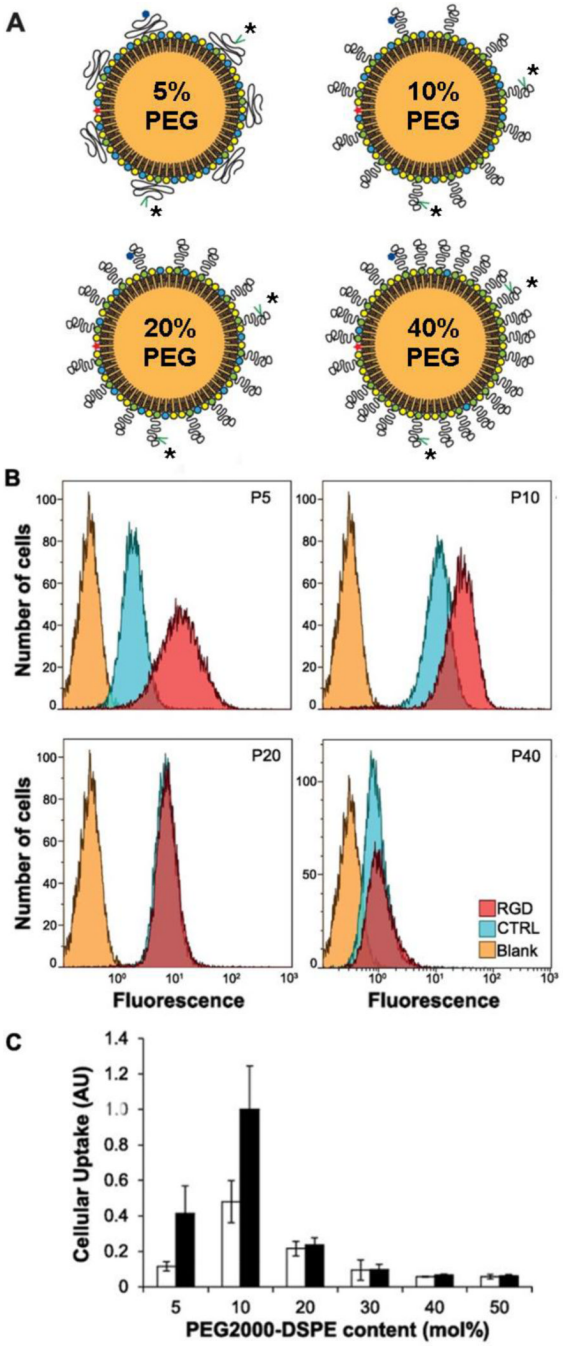


**Fig. 6.**

The effect of PEG density on the targeted uptake of labeled nano-emulsions ($d_h$ ~100 nm). (A) PEG chains adopt mushroom-like conformations at low density (5 mol%) to provide a semi-permeable layer, but have extended conformations at higher densities; * = RGD ligand. (B,C) Flow cytometry reveals that ligand-enhanced uptake is observed for RGD-labeled nano-emulsions with low PEG chain density, but ligand-mediated and overall cell uptake are both diminished for carriers with higher chain densities. © 2012 American Chemical Society (reprinted with permission) [120].

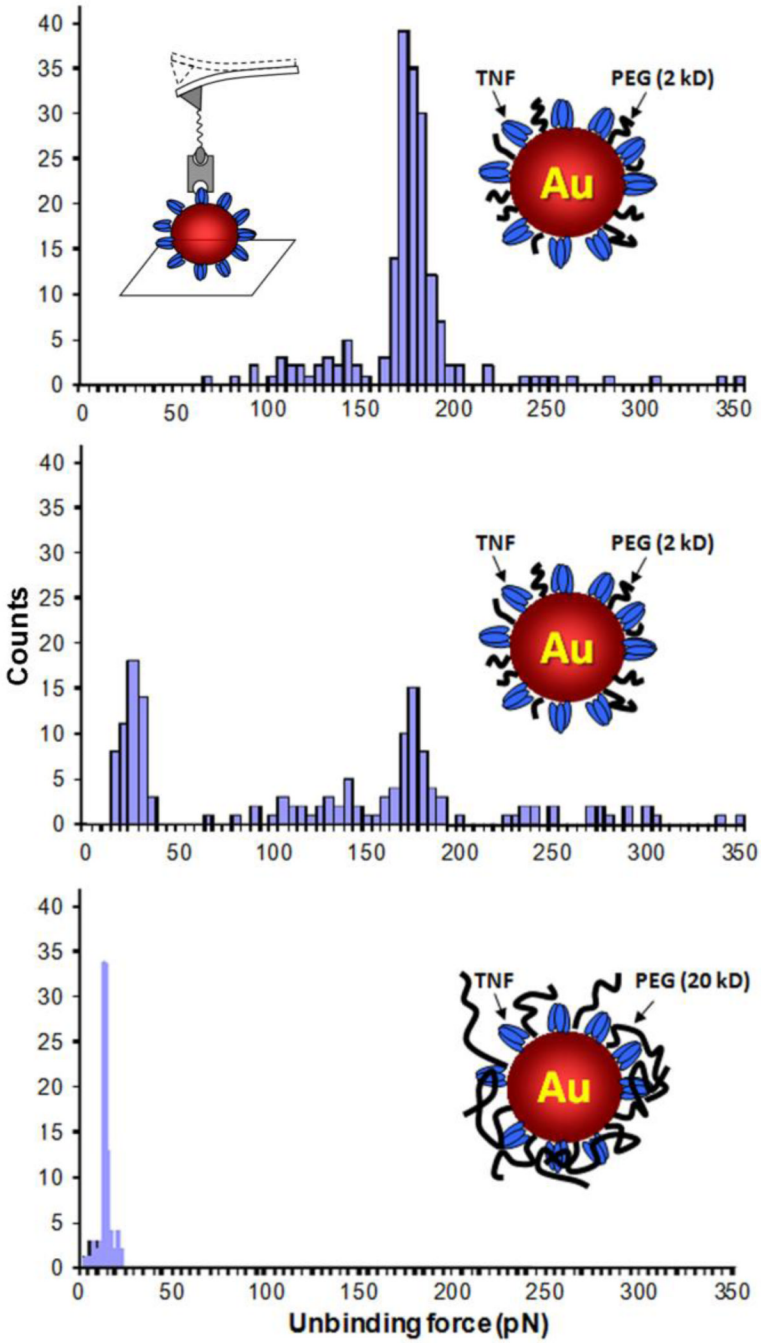


**Fig. 7.**

Ligand density on antigen-labeled Au nanoparticles with co-adsorbed PEG, characterized by an antibody-functionalized AFM probe tip (*inset, upper left*). As the PEG size increases, the number of measureable ligand–receptor interactions decreases ($F$~180 pN), with a commensurate rise in nonspecific substrate–tip interactions ($F$~20 pN).

## Table 1

Selected Examples of Nanomedicines for Cancer Treatment (Approved or in Clinical Development)

| Carrier type (size) | Activity or active ingredients | Nanomedicine (drug name) | Approval/Clinical testing | Refs. |
|---|---|---|---|---|
| Liposome (100 nm) | Doxorubicin | Doxil® | Approved for multiple cancers | [8] |
| Liposome (100 nm) | Daunorubicin citrate | DaunoXome® | Approved for Kaposi's sarcoma | [15] |
| CM-dextran- $Fe_3O_4$ NPs (40–60 nm) | Imaging agent (MRI contrast) | Resovist® | Approved for liver/HCC imaging | [16] |
| Colloidal albumin (123 nm) | Paclitaxel | Abraxane® | Approved for metastatic breast cancer | [9,10] |
| Liposome (120 nm) | Vincristine sulfate | Marqibo® | Approved for acute lymphoblastic leukemia (ALL) | [11] |
| Aminosilane-coated SPIOs (16 nm) | magnetic hyperthermia | NanoTherm® | Approved (EU) for glioblastomas | [17,18] |
| Polymer-drug conjugate | Paclitaxel | CT-2103 (Xyotax) | Phase III: ovarian, NSCLC | [19] |
| PEG micelle | Irinotecan | NKTR-102 | Phase III: breast, colorectal Phase II: ovarian | [20] |
| liposome (100 nm) | Doxorubicin, thermal release | ThermoDox® | Phase III: liver/HCC Phase II: metastatic cancers | [21] |
| PEG-PLA micelle | Paclitaxel | Genexol-PM | Phase III: breast; Phase II: bladder, pancreatic, lung (NSCLC), ovarian | [22,23] |
| Liposome (107 nm) | Cytarabine, daunorubicin | CPX-351 | Phase IIB: acute myeloid leukemia (AML) | [24,25] |
| Retrovector | Cyclin G1 proto-oncogene | Rexin-G™ | Phase II: breast, pancreatic, sarcomas | [26] |
| Cyclodextrin-PEG micelle (30 nm) | Camptothecin | CRLX-101 (formerly IT-101) | Phase II, lung (NSCLC), ovarian Phase I, renal / RCC | [27] |
| Polymer conjugate | camptothecin | XMT-1001 | Phase IB, solid tumors | [28] |
| Cyclodextrin-PEG micelle (100 nm) | siRNA (anti-RRM2) | CALAA-01 (Cyclosert) | Phase I, solid tumors | [29,30] |
| PEG-PLGA micelle | Docetaxel | BIND-014 | Phase I, metastatic cancers | [31,32] |
| Gold nanoparticle (27 nm) | Tumor Necrosis Factor | CYT-6091 (Aurimmune) | Phase I, solid tumors | [33] |
| Nano-dispersion | Paclitaxel | PICN | Phase I, solid tumors | [34] |
| $HfO_2$ nanoparticles | X-ray activation (radiotherapy) | NBTXR3 | Phase I, sarcomas | [35] |
| Gold nanoshells (150 nm) | NIR irradiation (thermal ablation) | Auroshell | Pilot (Phase 0), Head/neck cancers | [36] |
| PEG-coated $SiO_2$(7 nm) | imaging agent (PET) | C-dots | IND approval | [37] |